Journal of Solid State Chemistry 182 (2009) 1438–1442

Contents lists available at ScienceDirect

Journal of Solid State Chemistry

journal homepage: www.elsevier.com/locate/jssc

Metal–nonmetal transition in the sphalerite-type solid solution $[ZnSnSb_2]_{1-x}[2(InSb)]_x$

Andreas Tengå [a], F. Javier Garcia-Garcia [b], Yang Wu [c], N. Newman [d], Ulrich Häussermann [c,*]

[a] Inorganic Chemistry, Stockholm University, SE-10691 Stockholm, Sweden
[b] Lehrstuhl für Festkörperchemie, Institut für Physik, Universität Augsburg, D-86159 Augsburg, Germany
[c] Department of Chemistry and Biochemistry, Arizona State University, Tempe, AZ 85287-1604, USA
[d] School of Materials, Arizona State University, Tempe, AZ 85287-8706, USA

ARTICLE INFO

Article history:
Received 12 February 2009
Received in revised form
16 March 2009
Accepted 21 March 2009
Available online 5 April 2009

Keywords:
Metal–nonmetal transition
Sphalerite structure
Indium antimonide
Solid solution

ABSTRACT

Samples of the solid solution $[ZnSnSb_2]_{1-x}[2(InSb)]_x$ have been prepared over the whole range of composition by tin flux synthesis. The lattice parameter of the sphalerite-type average structure varies linearly between that of the end members $ZnSnSb_2$ and InSb, $a = 6.2849(2)$ and 6.4776(15), respectively. Electron diffraction shows different kinds of structured diffuse scattering for Zn and In rich samples, respectively. The former is attributed to compositional short range ordering, the latter to thermally excited phonon modes. A metal–nonmetal transition takes place between the compositions $x = 0.8$ and $x = 0.9$.

1. Introduction

Among the III–V semiconductors InSb has the smallest band gap ($E_g = 0.17$ eV at room temperature) and is distinguished by a high photon absorption efficiency and an extraordinarily high mobility of charge carriers: 78 000 and 750 $cm^2 V^{-1} s^{-1}$ at 77 K for electrons and holes, respectively, which is 50 and 5 times greater than those of Si [1,2]. These properties make InSb an important material in infrared detector and magnetoresistivity sensing technology [3,4]. Exchanging trivalent In for the equiatomic II–IV mixture Zn–Sn results in the II–IV-V_2 compound $ZnSnSb_2$ which is a strongly degenerate *p*-type semiconductor with a metallic temperature dependence of the resistivity [5–7]. Compared to InSb the mobility of charge carriers (holes) is reduced by an order of magnitude while the carrier concentration is increased by 3–4 orders of magnitude (from 2×10^{16} to approximately 10^{20} cm^{-3}) [8–10].

In this work we want to investigate whether an isoelectronic solid solution $[ZnSnSb_2]_{1-x}[2(InSb)]_x$ displays a continuous metal–nonmetal transition. Apparently the system $[ZnSnSb_2]_{1-x}[2(InSb)]_x$ has been investigated earlier in the course of finding new thermoelectric materials that possess electrical properties similar to InSb, but at the same time have greatly reduced thermal conductivites through alloying [11]. Reported results, however, are not conclusive. While the work of Voltsekhivs'kii [12] suggests solid solution behavior over the whole range of compositions, *x*, more recently Khalilov et al. [13] stated that solid solutions can only be obtained for $0.7 < x < 1.0$, and that already very small amounts of $ZnSnSb_2$ (around 0.1 mol%) incorporated in InSb cause a transition from semiconductor to metallic behavior. As a peculiarity, $ZnSnSb_2$ decomposes peritectically at 633 K and can only be prepared from reaction mixtures containing a large excess of Sn, i.e. where Sn is employed as reactive flux [10,14]. Consequently, our synthesis approach was to use a Sn flux for the preparation of $[ZnSnSb_2]_{1-x}[2(InSb)]_x$ including the end member InSb ($x = 1$).

2. Experimental

Sample preparation: Starting materials were shots of Zn (99.99%, 1–3 mm), powder of Sb (99.9%, ~100 mesh), shots of Sn (99.999%), and shots of In (99.99%, 2–5 mm) purchased from Sigma-Aldrich. Reaction mixtures (3 g batches) were aimed to obtain a flexible ratio for Zn/In while keeping the concentration for Sn and Sb constant and weighed according to the formula $[(1-x)ZnSnSb_2+(2x)InSb+(4+x)Sn]$. Two sample series were prepared: $x = 0.1, 0.2, 0.3, 0.4, 0.5, 0.6, 0.7, 0.8, 0.9, 1.0$ at Arizona State University ("ASU" series) and $x = 0.4, 0.5, 0.6, 0.7, 0.8, 0.9, 1.0$ at Stockholm University ("SU" series). For both series mixtures of the pure elements were pressed into pellets and loaded into specially prepared evacuated fused silica tubes [15]. These tubes contained

* Corresponding author. Fax: +1 480 965 2747.
E-mail address: Ulrich.Haussermann@asu.edu (U. Häussermann).

0022-4596/$ - see front matter © 2009 Elsevier Inc. All rights reserved.
doi:10.1016/j.jssc.2009.03.015

the pellet at the bottom and a layer of coarsely crushed quartz glass fixed by a plug of quartz wool at the top. Evacuated and sealed ampoules were placed in a silica wool insulated reaction container made of stainless steel, which was subsequently placed in a furnace. The reaction mixture was first heated to 923 K for 24 h to ensure complete melting of the metals. During this time containers were periodically shaken. Thereafter, the temperature was lowered at a rate of 50 K/h to 623 K, and subsequently at a rate 1 K/h until a temperature of 523 K was reached. At this temperature the product was separated from the liquid excess metal mixture by centrifugation.

Sample characterization: Powder X-ray diffraction patterns were collected on a Siemens D5000 diffractometer (ASU sample products) and on a Panalytical X'Pert MPD diffractometer (SU sample products), both operated with Cu$K\alpha$ radiation. Lattice parameters were obtained from least-squares refinement of measured and indexed lines of the powder diffractograms [16]. The composition of the ASU sample products was analyzed on polished specimens embedded in an epoxy resin by electron probe microanalysis (EPMA) in a JEOL JXA-8600 microscope operated at 15.0 kV and 30.0 nA. Elemental metals were used as standards for Zn, Sb and Sn, while InSb was used for In, respectively. The composition of the SU sample products was analyzed by energy disperse X-ray spectrometry (EDX) in a JEOL JSM 7000F equipped with a EDX detector (Oxford Instruments, EDX system INCA X-sight with INCA software). Specimens were glued on a silicon wafer and polished by argon ion milling. X-rays were recorded with an accelerating voltage of 15 kV. The ZAF correction procedure was employed for quantitative composition determination in both types of analyses. Specimens (ASU sample products) for transmission electron microscopy studies were prepared by grinding crystals under ethanol. Some drops of the resulting dispersion were put onto holey carbon coated copper grids. These grids were examined in a JEOL JEM 2100F operated at 200 kV. This microscope is attached with an EDAX detector for compositional analysis of the samples by X-ray energy-dispersive spectrometry.

Resistivity measurements: The electrical resistivity of $[ZnSnSb_2]_{1-x}[2(InSb)]_x$ was measured on a Physical Property Measurement System (PPMS) from Quantum Design using a four-point probe in-line configuration. The compositions $x = 1.0$, 0.9, 0.8, 0.7, 0.6, and 0.5 were considered (ASU sample products). The specimen for $x = 1$ corresponded to a crystal obtained from the flux reaction that was shaped into a bar with dimensions $1.25 \times 0.90 \times 0.25$ mm, the remaining specimens were prepared by compacting powdered samples at 2 GPa in a multi-anvil pressure apparatus. This afforded cold pressed specimens in a uniform cylinder shape with dimensions 4.48 mm in diameter, 2.48 mm in length and a density corresponding to the theoretical one. Gold bonding wires (0.00125 mm) were painted on the sample and electrodes on the resistivity puck using an air-drying silver paint (Demetron D200) for contacts. The puck was subsequently loaded into the PPMS chamber and then evacuated and sealed for the measurement. A constant current of up to 1 mA was applied and the resistance recorded from 10–350 K and 350–10 K (one heating/cooling cycle) at a rate of 1 K/min.

3. Results and discussion

The crystal structure of InSb corresponds to the cubic sphalerite (or zincblende) type (space group $F\bar{4}3m$, $Z = 4$) while $ZnSnSb_2$ adopts the tetragonal chalcopyrite structure (space group $I\bar{4}2d$, $Z = 4$). The chalcopyrite structure represents a tetragonal superstructure of the sphalerite structure where the ordered arrangement of II and IV-type atoms causes a doubling of the c unit cell parameter (Fig. 1) [11]. However, the chalcopyrite

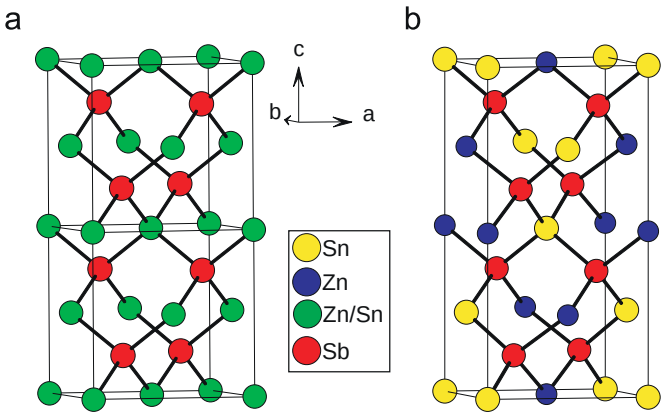

Fig. 1. Structures of cubic sphalerite (a) and tetragonal chalcopyrite (b).

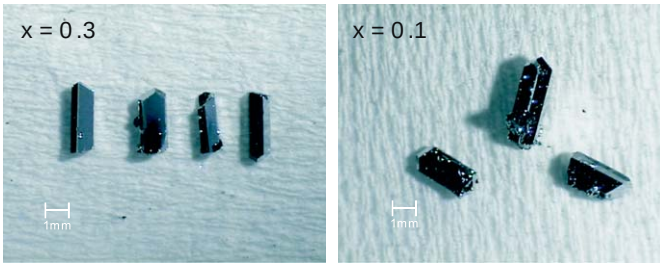

Fig. 2. Photographs of crystals from samples $[ZnSnSb_2]_{0.7}[2(InSb)]_{0.3}$ (left) and $[ZnSnSb_2]_{0.9}[2(InSb)]_{0.1}$ (right).

superstructure for $ZnSnSb_2$ is very difficult to detect. The structural parameters are very close to the ideal values ($c/a = 2.0$ and $x_{Sb} = 1/4$) and the tetragonal symmetry is primarily the result of Zn/Sn ordering. Recent electron microscopy studies have shown that chalcopyrite-type $ZnSnSb_2$ is intricately twinned and consists of domains with sizes below 100 Å [13]. At temperatures between 500 and 515 K $ZnSnSb_2$ undergoes an order–disorder transition to the sphalerite structure where Zn and Sn atoms are randomly distributed [14].

Tin flux synthesis affords mm-sized crystals of the solid solution $[ZnSnSb_2]_{1-x}[2(InSb)]_x$ over the whole range of composition (Fig. 2). As expected, X-ray powder patterns for the alloys exhibit exclusively reflections corresponding to the cubic sphalerite structure. The lattice parameter interpolates linearly between the end-members $ZnSnSb_2$ and InSb as a function of the In composition, in accord with Vegard's law (Fig. 3, Tables 1 and 2) [17]. The lattice parameter for Sn-flux synthesized InSb is 6.478 Å, which agrees with the literature value [2]. Electron probe microanalysis shows that Sn is not incorporated in InSb, $x = 1$ (Table 1). For the alloy samples, EPMA indicates that they are compositionally homogeneous but reveal systematic deviations from the target composition, which assumes the substitution pattern II/IV → 2 III. For $x = 0.9$–0.6 the Zn concentration appears higher than the Sn concentration. At the same time the valence electron concentration calculated from the total composition remains 4 per atom which implies that the excess of Zn over Sn is electronically compensated by a higher concentration of V-Sb and/or III-In. For $x = 0.5$ the Zn and Sn concentrations are equal, in agreement with the expected substitution pattern. For the samples $x = 0.4$, 0.3, 0.2, and 0.1 the Zn concentration becomes smaller than that of Sn, and this is balanced by a lower concentration of V-Sb and/or III-In. However, for $x = 0.2$ and 0.1 valence electron concentrations as calculated from the total composition start to deviate from 4 per atom.

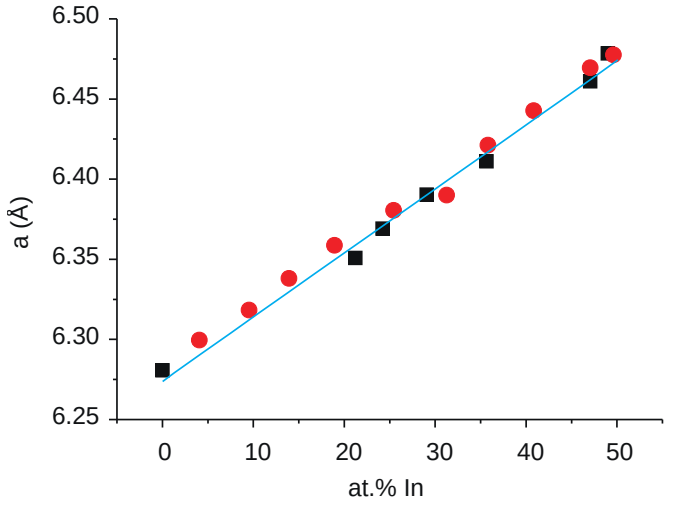

Fig. 3. The cubic lattice parameter a of $[ZnSnSb_2]_{1-x}[2(InSb)]_x$ vs the In concentration (at.%). The different symbols represent data of two different sample series. The line is a linear fit based on both sets of data.

Table 1
Cubic lattice parameter and EPMA determined composition for $[ZnSnSb_2]_{1-x}[2(InSb)]_x$; "ASU" sample series.

x	a (Å)	Sb	In	Sn	Zn	vec
1	6.4776(15)	50.25±0.38	49.6±0.23	0.02±0.02	0	4.001
0.9	6.4696(8)	50.83±0.18	47.06±0.22	0.33±0.14	1.76±0.18	4.002
0.8	6.4427(5)	50.69±0.31	40.84±0.25	3.63±0.25	4.84±0.15	3.997
0.7	6.4213(7)	50.42±0.16	35.81±0.54	6.51±0.29	7.3±0.23	4.002
0.6	6.3901(7)	50.2±0.09	31.25±0.83	8.97±0.56	9.57±0.33	3.998
0.5	6.3806(6)	49.75±0.22	25.42±0.65	12.36±0.47	12.47±0.30	3.994
0.4	6.3587(8)	49.07±0.12	18.92±0.82	16.92±0.18	15.38±0.29	4.006
0.3	6.3381(4)	49.97±0.48	13.92±0.52	18.13±0.67	17.83±0.46	3.998
0.2	6.3184(3)	48.41±0.51	9.53±0.24	22.07±0.20	19.99±0.33	3.989
0.1	6.2996(2)	47.21±0.36	4.06±0.13	26.06±0.54	22.68±0.19	3.978
0[a]	6.2849(2)					

vec = electron concentration per atom according to the compositional analysis.
[a] According to Ref. [7]

Table 2
Cubic lattice parameter and EDX determined composition for $[ZnSnSb_2]_{1-x}[2(InSb)]_x$; "SU" sample series.

x	a (Å)	Sb	In	Sn	Zn	vec
1	6.4785(1)					
0.9	6.461(5)	50.8±0.54	47.06±1.07	0.55±0.51	1.59±0.65	4.006
0.7	6.4111(4)	50.38±0.89	35.64±0.99	6.57±0.93	7.4±1.04	3.999
0.6	6.3904(6)	49.7±0.74	29.07±0.97	10.34±0.92	10.89±0.74	3.989
0.5	6.3692(4)	50.21±0.54	24.21±0.87	12.08±0.95	13.5±0.82	3.990
0.4	6.3508(6)	51.18±0.60	21.22±0.99	14.53±0.96	13.07±0.60	4.034

vec = electron concentration per atom according to the compositional analysis.

The compositional variations suggest that the microscopic structure of alloys $[ZnSnSb_2]_{1-x}[2(InSb)]_x$ is more complicated than the simple picture of a sphalerite structure with Sb atoms occupying one position and a random distribution of Zn/Sn/In atoms on the other. Also, the question arises whether for low values x alloys $[ZnSnSb_2]_{1-x}[2(InSb)]_x$ actually crystallize with the chalcopyrite structure and a structural change to the sphalerite structure occurs with increasing x. In order to study these issues we performed electron diffraction experiments in the transmission electron microscope for the complete range of composition. These experiments revealed the set of basic reflections for the sphalerite-type structure in all samples. The reflection conditions are $F(hkl) = 0$ unless $h+k$, $h+l$, $k+l = 2n$, in agreement with the $F\bar{4}3m$ space group for this structure type. However, highly structured diffuse scattering is also present, with varying intensity. Hence, careful tilting experiments in the microscope were carried out and the results are compiled in Fig. 4. In (a), (c) and (e) the $<001>$ zone axis electron diffraction patterns recorded for $x = 0.9$, $x = 0.2$, and $x = 0.4$ samples, respectively, are presented. The corresponding patterns after tilting the crystals a few degrees away from the exact Bragg condition are shown in (b), (d) and (f).

The diffraction patterns for $[ZnSnSb_2]_{0.1}[2(InSb)]_{0.9}$, $x = 0.9$, show the presence of highly structured diffuse scattered intensity which apparently form lines running along every direction $<110>^*$ of the sphalerite structure (Fig. 4a and b). The intensity is increased towards the edge of the diffraction pattern suggesting a displacive origin for this scattered intensity distribution. After tilting the crystals and recording several diffraction patterns in all major zone axes, we conclude that the lines of diffuse scattering shown in Fig. 4a are actually part of sheets of diffuse scattering. This feature is present in samples for all compositions, but when x decreases (i.e. samples become more Zn rich) additional, and seemingly not correlated, diffuse scattered intensity appears.

The diffraction patterns shown in Figs. 4c and d were recorded for $[ZnSnSb_2]_{0.8}[2(InSb)]_{0.2}$, $x = 0.2$, and indicated with arrows are some weak and not well defined reflections. They are part of continuous diffuse scattering intensity which is starting condensing out into Bragg reflections. These reflections can be indexed with a modulation wave vector of the type $\mathbf{q} \approx \pm 1/4 <024>^*$, which coincides with the lattice of the chalcopyrite superstructure [14]. Note that in the diffraction patterns for $x = 0.2$ the sheets of diffuse scattering observed for $x = 0.9$ (Figs. 4a and b) are also present, even though with much less intensity. Corresponding experiments for the sample $[ZnSnSb_2]_{0.6}[2(InSb)]_{0.4}$, $x = 0.4$, clearly show the same characteristics (Fig. 4e and f), while for $x = 0.5$ the second type of diffuse scattering intensity is absent (not shown).

To explain the two kinds of diffuse scattering we note that the diffuse intensity distribution in the In rich samples is equivalent to that previously reported by Withers et al. for ZnS [18]. There, the presence of structured diffuse scattering was interpreted to originate from low-frequency phonon modes propagating along reciprocal space directions perpendicular to each of the six {110} real space directions of the sphalerite structure. It has been further postulated that such low-frequency phonon modes should be an intrinsic property of the corner connected tetrahedral structure of sphalerite. Indeed, we observe this kind of diffuse scattering also in the binary InSb ($x = 1$) sample and therefore it is not associated with alloying. In a resent paper by Rosenauer et al. thermal diffuse scattering has been simulated for InSb and these simulations agree perfectly with our experiments [19]. The modulated diffuse scattering observed for Zn rich samples ($x<0.5$) is attributed to compositionally driven short range ordering aimed to ensure locally valence electron concentrations of 4 per atom. This may lead to a microscopic segregation of domains of $ZnSnSb_2$ in quaternary alloy samples for $x<0.5$.

Fig. 5 compiles the results of the resistivity measurements for specimens $x = 1$, 0.9, 0.8, 0.7, 0.6, and 0.5. The InSb ($x = 1$) sample displays resistivity values around 1.4 Ω cm at l0 K, which decrease to about 0.4 Ω cm at room temperature. These values are high, but typically found for hole conducting specimens [20–22]. Depending on the kind of charge carriers and their concentration, resistivities of InSb at low temperatures (i.e. below room temperature) differ by several orders of magnitudes and show

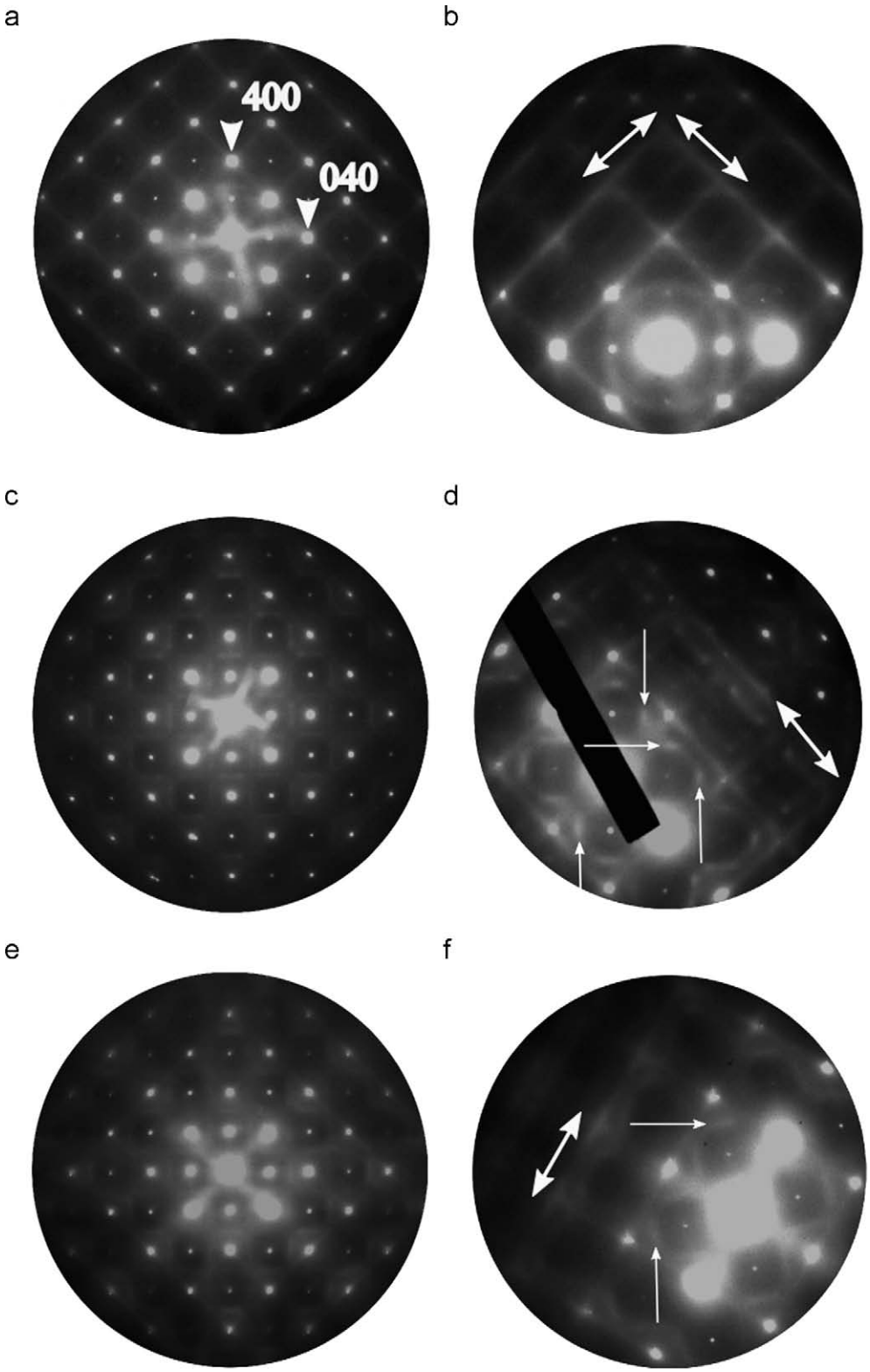

Fig. 4. ⟨001⟩ Zone axis electron diffraction patterns recorded for ("ASU") samples $[ZnSnSb_2]_{1-x}[2(InSb)]_x$ $x = 0.9$ (a), $x = 0.2$ (b), and $x = 0.4$ (c). In (b), (d) and (f) the corresponding tilting experiments are shown. Double-head arrows indicate lines of (composition-independent) diffuse scattering running along ⟨110⟩* and arrows the positions of the superstructure reflections ($\mathbf{q} \approx \pm 1/4$ ⟨024⟩*) condensing out from additional, composition-dependent, diffuse scattering intensity.

only weak temperature dependence. At higher temperatures (250–400 K) resistivities converge into the temperature dependence of intrinsic conductivity. For our sample the temperature range for intrinsic conductivity is not reached, and its behavior is similar to sample "p2" in Ref. [19]. The sample $x = 0.9$ still shows semiconductor behavior, although resistivity values have dropped by two orders of magnitude. Again temperatures up to 350 K do not seem to be sufficient to achieve intrinsic conductivity. For sample $x = 0.8$ the temperature dependence of the resistivity is changed to metallic like. However, ρ varies only little with

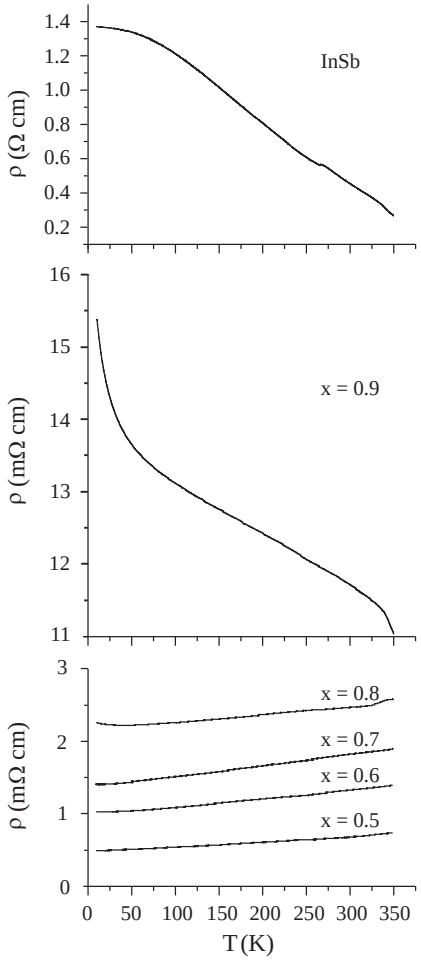

Fig. 5. Resistivity ρ of $[ZnSnSb_2]_{1-x}[2(InSb)]_x$ for $x = 1$, 0.9, 0.8, 0.7, 0.6, and 0.5 ("ASU" sample specimens).

temperatures and values are typical of a poor metal or a degenerate semiconductor (2–3 mΩ cm). The samples $x = 0.7$, 0.6, and 0.5 show virtually the same temperature dependency and resistivity values become increasingly lower. For $x = 0.5$ they are in a range of 0.5–0.6 mΩ cm. For $ZnSnSb_2$ earlier measurements revealed room temperature values around 0.3 mΩ cm [7,14]. It is reasonable to assume that the solid solution samples are *p*-type conductors, because our Sn-flux prepared InSb ($x = 1$) shows the characteristics of a *p*-type specimen [20–22] and $ZnSnSb_2$ is known to be a *p*-type conductor [14].

In conclusion, we find a continuous change of the resistivity in the solid solution $[ZnSnSb_2]_{1-x}[2(InSb)]_x$, with a metal–nonmetal transition occurring between $x = 0.8$ and 0.9. This result is in sharp contrast to the earlier investigation by Khalilov et al. [13] reporting that already very small concentrations of $ZnSnSb_2$ (at the doping level) cause InSb to display a metallic resistivity behavior. Our results suggest that it may be worthwhile to revisit the thermoelectric properties of $[ZnSnSb_2]_{1-x}[2(InSb)]_x$. As earlier demonstrated, metallic $ZnSnSb_2$ has a rather low thermopower [14], while *p*-type InSb with a high resistivity shows values above 100 μV/K at room temperature [23]. Resistivity and thermopower of samples with compositions between $x = 0.8$ and 0.9 may represent a good compromise, and such compositions could display the highest thermoelectric figure of merit within this solid solution.

4. Conclusions

Compositionally homogeneous samples of the solid solution $[ZnSnSb_2]_{1-x}[2(InSb)]_x$ can be prepared over the whole range of composition by Sn flux synthesis. According to powder X-ray diffraction the alloys crystallize with the cubic sphalerite structure and the lattice parameter changes linearly as a function of the composition, *x*. Electron diffraction reveals structured diffuse scattering for $x < 0.5$, indicative of compositional short range ordering and consequently chalcopyrite domain formation. Thermal diffuse scattering probably inherent to the sphalerite structure is observed for the whole range of compositions. Samples with low *x* display a metallic conductivity behavior which changes into semiconductor behavior between $x = 0.8$ and 0.9. These samples may reveal interesting thermoelectric properties.

Acknowledgment

This research has been supported by National Science Foundation grant DMR-0638826. We are grateful to Dr. Gordon Moore (ASU) and Dr. Kjell Jansson (Stockholm Univeristy) for assistance with WDX and EDX compositional analysis, respectively.

References

[1] K.F. Hulme, J.B. Mullin, Solid State Electron 5 (1962) 211.
[2] R.G. Breckenbridge, R.F. Blunt, W.R. Hosler, H.P.R. Frederikse, J.H. Becker, W. Oshinsky, Phys. Rev. 96 (1954) 571.
[3] R. Szweda, III–Vs Rev. Semicond. Mag. 17 (2004) 32.
[4] I. Kimukin, N. Biyikli, T. Kartaloglu, O. Aytür, E. Ozbay, IEEE J. Sel. Top. Quant. 10 (2004) 766.
[5] N.A. Goryunova, B.V. Baranov, V.S. Grigoreva, L.V. Kradinova, V.A. Maksimova, V.D. Prochukhan, Izv. Akad. Nauk SSSR, Neorg. Mater. 4 (1968) 1060.
[6] A.A. Vaipolin, L.V. Kradinova, V.D. Prochukhan, Sov. Phys. Cryst. 15 (1971) 703.
[7] L.V. Kradinova, T.I. Voronona, Phys. Status Solidi 32 (1969) K173.
[8] V.N. Ivakhno, L.V. Kradinova, V.D. Prochukhan, Sov. Phys. Semicond. 3 (1970) 913.
[9] Y.I. Polygalov, Y.M. Basalaev, M.L. Zolotarev, A.S. Poplavnoi, Sov. Phys. Semicond. 23 (1989) 173.
[10] W. Scott, J. Appl. Phys. 44 (1973) 5165.
[11] J.L. Shay, J.H. Wernick, Ternary Chalcopyrite Semiconductors: Growth, Electronic Properties, and Applications, Pergamon Press, New York, 1975.
[12] O.V. Voltsekhivskii, A.M. Gorkii, Ukr. Fiz. Zh. 9 (1964) 796.
[13] M.I. Aliev, K.Y. Khalilov, Mater. Dokl. Nauch.-Tekh. Konf. Kishinev. Politekh. Inst., 2nd Kishinev (1966) 135.
[14] A. Tengå, F.J. García García, A.S. Mikhaylushkin, B. Espinosa-Arronte, M. Andersson, U. Häussermann, Chem. Mater. 17 (2005) 6080.
[15] M. Boström, S. Hovmöller, J. Solid State Chem. 153 (2000) 398.
[16] P.-E. Werner, Ark. Kemi 31 (1969) 513.
[17] L. Vegard, Z. Phys. 5 (1921) 17.
[18] R.L. Withers, T.R. Welberry, A. Pring, C. Tenailleau, Y. Liu, J. Solid State Chem. 178 (2005) 655.
[19] A. Rosenauer, M. Schowalter, J.T. Titantah, D. Lamoen, Ultramicroscopy 108 (2008) 1504.
[20] H. Weiss, Z. Naturforsch. A 8 (1953) 463.
[21] D.N. Nasledov, A.I. Khalilov, Sov. Phys. Tech. Phys. 1 (1956) 3.
[22] S. Hishiki, Y. Kogetsu, I. Kanno, H. Yamana, Jpn. J. Appl. Phys. 46 (2007) 5030.
[23] E. Majkova, J. Cervenak, J. Krempasky, P. Duhaj, Phys. Status Solidi B 153 (1989) K147.